universe

MDPI

Article

Investigating Alfvénic Turbulence in Fast and Slow Solar Wind Streams

Raffaella D'Amicis [1,*], Denise Perrone [2], Marco Velli [3], Luca Sorriso-Valvo [4,5], Daniele Telloni [6], Roberto Bruno [1] and Rossana De Marco [1]

[1] INAF-Institute for Space Astrophysics and Planetology, 00133 Rome, Italy; roberto.bruno@inaf.it (R.B.); rossana.demarco@inaf.it (R.D.M.)
[2] Italian Space Agency (ASI), 00133 Rome, Italy; denise.perrone@asi.it
[3] Department of Earth, Planetary and Space Sciences, University of California Los Angeles, Los Angeles, CA 90095, USA; mvelli@ucla.edu
[4] Istituto per la Scienza e Tecnologia dei Plasmi, Consiglio Nazionale delle Ricerche, 70126 Bari, Italy; lucasorriso@gmail.com
[5] Swedish Institute of Space Physics, Ångström Laboratory, 75237 Uppsala, Sweden
[6] INAF-Osservatorio Astrofisico di Torino, 10025 Pino Torinese, Italy; daniele.telloni@inaf.it
* Correspondence: raffaella.damicis@inaf.it

Abstract: Solar wind turbulence dominated by large-amplitude Alfvénic fluctuations, mainly propagating away from the Sun, is ubiquitous in high-speed solar wind streams. Recent observations performed in the inner heliosphere (from 1 AU down to tens of solar radii) have proved that also slow wind streams show sometimes strong Alfvénic signatures. Within this context, the present paper focuses on a comparative study on the characterization of Alfvénic turbulence in fast and slow solar wind intervals observed at 1 AU where degradation of Alfvénic correlations is expected. In particular, we compared the behavior of different parameters to characterize the Alfvénic content of the fluctuations, using also the Elsässer variables to derive the spectral behavior of the normalized cross-helicity and residual energy. This study confirms that the Alfvénic slow wind stream resembles, in many respects, a fast wind stream. The velocity-magnetic field (v-b) correlation coefficient is similar in the two cases as well as the amplitude of the fluctuations although it is not clear to what extent the condition of incompressibility holds. Moreover, the spectral analysis shows that fast wind and Alfvénic slow wind have similar normalized cross-helicity values but in general the fast wind streams are closer to energy equipartition. Despite the overall similarities between the two solar wind regimes, each stream shows also peculiar features, that could be linked to the intrinsic evolution history that each of them has experienced and that should be taken into account to investigate how and why Alfvénicity evolves in the inner heliosphere.

Keywords: interplanetary medium; solar wind; magnetic field; turbulence; methods: data analysis

Citation: D'Amicis, R.; Perrone, D.; Velli, M.; Sorriso-Valvo, L.; Telloni, D.; Bruno, R.; De Marco, R. Investigating Alfvénic Turbulence in Fast and Slow Solar Wind Streams. *Universe* **2022**, *8*, 352. https://doi.org/10.3390/universe8070352

Academic Editor: Pablo S. Moya

Received: 6 May 2022
Accepted: 24 June 2022
Published: 27 June 2022

1. Introduction

Solar wind turbulence is often found to be Alfvénic, i.e., in addition to displaying well-developed power laws in frequency (first observed by [1]), a high degree of magnetic field (b)-velocity field (v) correlations corresponding to waves propagating away from the Sun [2,3] is observed, typically in fast wind streams. Being the solutions of the magnetohydrodynamics (MHD) equations, Alfvén waves are characterized not only by v-b correlations but also by almost constant number density and magnetic field magnitude. More in general, the condition of quasi-incompressibility results in relative density fluctuations (computed as the RMS of the proton number density, n_p, normalized to the average value), $\delta n_p/n_p$, smaller than the turbulent Mach number squared [4]. This comes directly from estimating the pressure fluctuations arising from the nonlinear interactions in the momentum equation and then assuming these fluctuations to be of the order of the density fluctuation times the

sound speed squared [5]. The turbulent Mach number has been evaluated as the ratio of the RMS value of velocity fluctuations, δv, and the sound speed, $c_s = (2\gamma k T_p / m_p)^{1/2}$, with γ the adiabatic index, set to 5/3 for the interplanetary plasma, k the Boltzmann constant, T_p the proton temperature and m_p the proton mass while factor 2 comes from taking the electron temperature equal to that for protons [6]. Moreover, for Alfvénic intervals, the RMS of the total magnetic field magnitude, δB, fluctuates less than the RMS of the vector field components, δb_i.

The Alfvénic content of the fluctuations is one of the differences distinguishing between fast and slow solar wind streams. Early studies showed that slow wind is characterized by more variable lower proton temperatures and higher density than the fast wind, which in turn is characterized by persistent particle distribution function thermal anisotropies [7]. Moreover, slow wind is usually described by more standard turbulence, characterized by power laws with Kolmogorov-type slopes [8], absence of outwardly propagating Alfvénic fluctuations, and larger density fluctuations [4]. However, [9] observed a peculiar slow solar wind at Helios 2 perihelion (around 0.29 AU), during the ascending phase of solar cycle 21, characterized by typical features observed in fast solar wind streams. Indeed, they found pronounced differential speeds between proton and alpha particle bulk flows and large proton temperature anisotropies along with the signature of Alfvénic fluctuations.

Alfvénic slow wind intervals were considered to be rare peculiar flows until measurements at the Lagrangian point L1 during solar maximum revealed a statistically significant occurrence of such streams [10]. The similarities with the fast wind were also investigated statistically based on a wide range of parameters at 1 AU at solar maximum [11,12] and were analyzed also at a solar minimum by studying the Helios data collected in the inner heliosphere [13,14]. As a consequence, the Alfvénic content of the fluctuations rather than the flow speed seems to be a good parameter to classify the solar wind ([15], and references therein). Moreover, the similar composition signatures found in both fast and Alfvénic slow wind [12] suggest a similar origin, that is coronal holes or more in general open field regions with strongly diverging and expanding field lines as the low-latitude coronal holes and the boundaries of the polar coronal holes, which are both regions of anomalous (greater than average) areal expansion of magnetic flux tubes near the Sun. Being a more detailed overview of the solar source of this solar wind regime out of scope, we redirect the reader to a recent review on the Alfvénic slow wind [15].

The previous studies have been confirmed by recent observations by Parker Solar Probe (PSP). During its first perihelion passage occurred in November 2018, PSP was located at a heliocentric distance around 0.16 AU and was embedded mainly in an Alfvénic slow wind except for brief periods [16–18]. Strong Alfvénic fluctuations were observed also in the other encounters, suggesting that Alfvénic fluctuations might dominate the nascent solar wind quite generally except for the immediate surroundings of the heliospheric current sheet.

More recently, Solar Orbiter also crossed an Alfvénic slow wind stream at a heliocentric distance of 0.64 AU [19], which was found to resemble a fast wind stream from many perspectives: from large-scale properties (e.g., the qualitative behavior of the speed profile), to small scales (e.g., the presence of waves with a well-defined magnetic helicity signature) and a similar solar source. In this regard, it is worth mentioning that the Alfvénic slow wind seems to be related to the presence of large-scale pseudostreamer configurations, that present a strong non-monotonic expansion of the open magnetic field lines. This would slow down the fast wind, setting the conditions for the development of the Alfvénic slow solar wind [20,21]. Whether both fast and slow wind originates from open field regions, something must account for the difference in speed of the two solar wind regimes. This is why the study of the Alfvénic slow wind may provide a better understanding of the more general problem of the origin and acceleration of the solar wind.

The Alfvénic content of solar wind fluctuations decreases with the heliocentric distance [22–27]. This evidence has been interpreted as an increase in the production

of the inward modes within those regions such as stream shears where some plasma instability is active. On the other hand, ref. [28] noticed that the decrease of Alfvénicity is closely related to magnetic field and/or density enhancements most of the time, relating this behavior to a lack of Alfvénicity in the fluctuations rather than the local generation of inward modes [29,30]. The radial evolution of Alfvénicity has been investigated using mainly Helios observations of fast and slow wind streams at different heliocentric distances in the inner heliosphere and more recently using PSP observations. Although slow wind can be quite Alfvénic closer to the Sun [9,16], the Alfvénic content of this solar wind regime is rapidly lost when moving to 1 AU [31,32]. As a consequence, observing an Alfvénic slow wind at 1 AU is both unexpected and uncommon and represents a good opportunity to understand the evolution of Alfvénicity in the inner heliosphere.

The aim of this study is to perform a comparative study between different Alfvénic streams (fast and slow) at 1 AU by means of relevant parameters to characterize Alfvénic fluctuations. This is extremely important for interpreting future observations of the same solar wind regime in future observations performed in the coming years. Indeed, we are approaching solar maximum which is characterized by a predominance of this solar wind regime [11,33].

2. Data Selection

The data analysis is based on on-board plasma moments from the Three-Dimensional Plasma and Energetic Particle Investigation (3DP) and magnetic field data from the Magnetic Field Investigation (MFI) on board Wind both at a 3 s resolution, when the spacecraft was in the solar wind at 1 AU. Although magnetic field measurements are available at higher resolution (92 ms), a constrain is given by the resolution of plasma moments computed on board which is indeed 3 s. Although plasma parameters suffer from instrumental discretization at this time scale, this has no impact on lower frequencies' power spectral density (as already discussed in [34]). We selected one representative (corotating) fast wind stream detected during the minimum of solar cycle 22 and three Alfvénic slow wind streams selected during the maximum of solar cycle 23 (see Table 1 for average bulk parameters). This is motivated by the fact that, although in previous studies e.g., [12], the fast wind used for comparison was selected at a maximum of solar activity because it was found close to the Alfvénic slow wind, it is more appropriate to compare the Alfvénic slow wind to more standard corotating fast wind streams frequently observed during solar minimum e.g., [31,33], characterized by more stable solar sources.

In this section, we compare the time series of the fast wind (labeled 'F') and those corresponding to the Alfvénic slow stream labeled 'AS1', taken as an example.

Table 1. Average bulk parameters of the solar wind bulk speed, V_{sw}; proton number density, n_p; proton temperature, T_p; magnetic field magnitude, B, within each selected interval. The different time windows, corresponding to the most Alfvénic part of the streams, are labeled 'F' (fast wind) or 'ASn' (Alfvénic slow wind with n = 1, 2, 3) and are indicated with a year and DoY (Day-of-Year) format.

Label	Year:DoY	V_{sw} [km/s]	n_p [cm^{-3}]	T_p 10^5 [K]	B [nT]
F	1995: 030.5–033.5	644	3.50	2.52	5.79
AS1	2002: 154.0–155.5	453	4.92	1.82	7.29
AS2	2001: 352.0–355.0	422	2.73	1.03	5.47
AS3	2000: 324.0–326.5	387	5.37	1.11	6.33

Figure 1 gives an overview of the fast (left) and Alfvénic slow wind (right). The different panels show the time series of relevant parameters: (**a**) and (**f**) solar wind bulk speed, V_{sw}; (**b**) and (**g**) v–b correlation coefficient (C_{vb}) computed using a sliding window at 30 min scale; (**c**) and (**h**) the ratio of the RMS of magnetic field fluctuations, δb_i and the RMS of the magnitude, δB; (**d**) and (**i**) the relative density fluctuations (**RMS** of n_p computed at 30 min scale normalized to the proton number density) $\delta n_p/n_p$ (black) and the turbulent Mach number squared $(\delta v/C_s)^2$ (shaded red); (**e**) and (**j**) the proton number density, n_p and the magnetic field magnitude, B. The RMS of all the above parameters were computed at 30 min scale which is a typical characteristic time where solar wind fluctuations show a strong Alfvénic character [35].

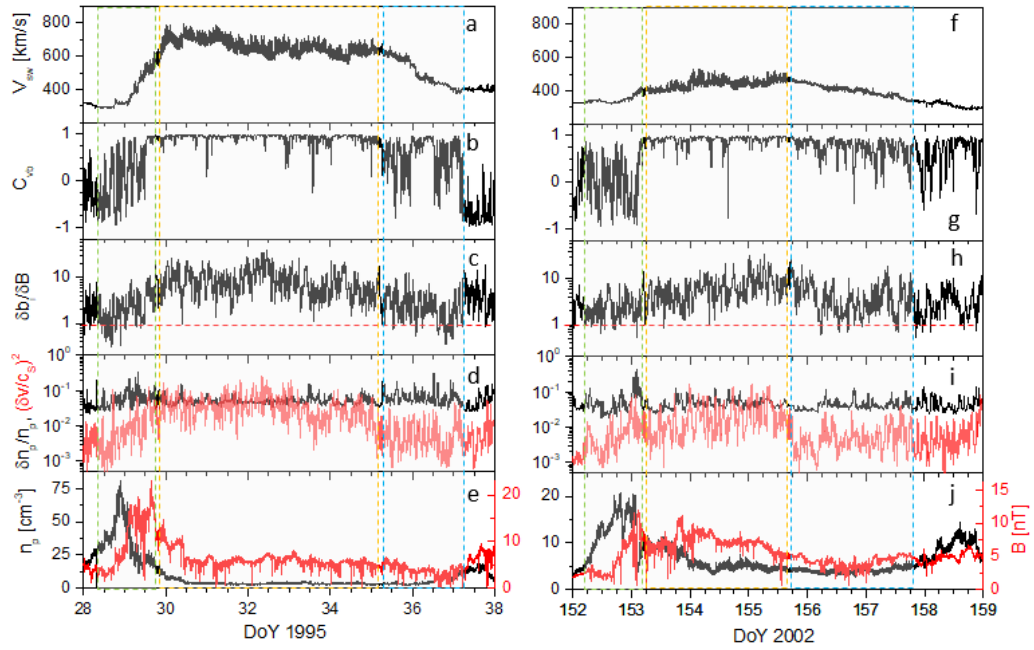

Figure 1. Time series of relevant parameters for a fast wind stream (left) and for an Alfvénic slow wind stream (right): (**a**,**f**) solar wind bulk speed, V_{sw}; (**b**,**g**) v-b correlation coefficient, C_{vb}; (**c**,**h**) relative magnetic field fluctuations respect to the fluctuations in the magnetic field magnitude, $\delta b_i/\delta B$; (**d**,**i**) relative density fluctuations, $\delta n_p/n_p$ (black) and the turbulent Mach number squared, $(\delta v/c_s)^2$ (shaded red); (**e**,**j**) number density, n_p (black) and magnetic field magnitude, B (red). The RMS of all the above parameters were computed at 30 min scale. The compression region, main portion of the stream and rarefaction region are indicated as green, orange and light blue dashed boxes, respectively.

In particular, the left side of Figure 1 displays a typical fast wind stream with well-recognizable features: (i) a compression region (DoY 28–30) characterized by an increase in magnetic field intensity and number density which is a result of the interaction between fast and slow solar wind that marks the transition between the two solar wind regimes; (ii) the main portion of the stream (from DoY 30 to 35) showing high speed and large amplitude Alfvénic fluctuations, as we will discuss in the paper; (iii) a rarefaction region (from DoY 35 to 36) where velocity decreases and fluctuations have smaller amplitude. The speed profile (panel a) within the main portion of the stream exhibits large velocity variations, called microstreams [36–38] attributed to the in situ signature of reconnection jets, due to newly emerging brightpoint loops present in the chromospheric network [39]. This stream can be compared to the fast wind described in [34], showing similar features but with a different length characterizing each sub-interval. This might be related to a different way the spacecraft crosses the stream or to the intrinsic features of each stream.

C_{vb} (panel b) is a measure of the degree of Alfvénicity and its value changes when moving across the three regions described above. Indeed, while the compression region ahead of the stream is characterized by uncorrelated velocity and magnetic field components (C_{vb} with fast oscillations from negative to positive values), the highest values of C_{vb} correspond to the main portion of the stream. The rarefaction region is again characterized by no v-b correlations (apart from the interval DoY 36–36.5 showing some v-b correlations). The polarity inversion occurring during the last day of the interval clearly marks the passage to another solar wind regime.

A prominent feature of Alfvénic fluctuations in the presence of quasi-incompressible conditions, as explained in the introduction. We verified these conditions in panels c, d, and e. In the main portion of the stream, the following evidences stand: (i) $\delta b_i/\delta B > 1$ with values oscillating around 10 and, sometimes, as high as 40; (ii) although $(\delta v/c_s)^2$ significantly fluctuates, during DoY 31.5–33 the condition $\delta n_p/n_p < (\delta v/c_s)^2$ is satisfied (by considering also that the scale is logarithmic). However, there is not a perfect correspondence with the highest values of C_{vb} or with the occurrence of condition (i); (iii) number density and magnetic field magnitude are quite constant. It is worth noting that in the interval DoY 33–34, C_{vb} is less stable and oscillates, $\delta b_i/\delta B$ decreases but still remaining > 1, while $\delta n_p/n_p$ becomes comparable with $(\delta v/c_s)^2$ or even larger, in contrast with expectations.

The right side of Figure 1 shows an example of Alfvénic slow solar wind with a non-Alfvénic slow wind preceding it. The Alfvénic slow wind displays a speed profile very similar to that of the fast wind being characterized by a compression region (DoY 152.25–153.25, although not as clear as in the fast wind case), followed by the main portion of the stream (DoY 153.25–155.75) and then a rarefaction region (DoY 155.75–157.75), as already pointed out by [12]. Obviously, the absolute value of the speed is lower than the one in a fast stream, ranging between 400 and 500 km/s. A similar wind profile is seen also in other Alfvénic slow wind streams (as the ones selected in this analysis) and for instance also in the case study described by [34]. However, the presence of the rarefaction region is not common to all the Alfvénic slow streams analyzed so far, probably due to the way the spacecraft crosses the different streams. This is an issue deserving further investigation.

Panel (f) shows large velocity variations similar to the fast wind in the interval DoY 153.25 to 155.75 delimiting quite well the most Alfvénic part of the stream (high values of C_{vb}, panel g). At the same time, $\delta b_i/\delta B > 1$ (panel h) in the same interval while, remarkably, $\delta n_p/n_p$ is comparable to $(\delta v/c_s)^2$, rather than being lower, but in a reduced interval, say from 154 to 155.5 (panel i) which corresponds also to the largest velocity variations. Panel j, on the other hand, shows a quite constant number density while the magnetic field magnitude is more variable but quite constant in the interval 154–155.5. After DoY 155.5 (corresponding to the rarefaction region), the velocity spikes disappear abruptly, along with a decrease in the v-b correlation decrease, of $\delta b_i/\delta B$ which approaches 1 and $\delta n_p/n_p$ much larger than $(\delta v/c_s)^2$.

Finally, we note that, for both fast (left panels of Figure 1) and Alfvénic slow wind (right panels of Figure 1) regimes, in the main part of the stream when the amplitude of the fluctuations is the largest, the magnetic field intensity (bottom panel) remains relatively stable; this is a consequence of the Alfvénicity of the fluctuations and the low level of B variations associated to it.

These features suggest a clear similarity between the fluctuations in the Alfvénic slow and fast wind. However, it is remarkable that the incompressible conditions seem to be weak in certain Alfvénic streams as we will discuss in Section 4.

The results of this preliminary analysis on the behaviour of C_{vb}, $\delta b_i/\delta B$ and $\delta n_p/n_p$ compared to $(\delta v/c_s)^2$ motivated us to select the intervals indicated in Table 1 for the analysis performed in the following section.

3. Spectral Analysis

To characterize velocity and magnetic field fluctuations, we perform spectral analysis. To better highlight the similarities and differences of streams with different bulk speeds and average magnetic field magnitude, we compute normalized power spectra in a way similar to [34,40] to obtain the relative amplitude of the fluctuations vs. frequency, normalized to their respective fields (e.g., $\delta V(f)/ < V >$ and $\delta B(f)/ < B >$ for relative velocity and magnetic field fluctuations, respectively). The amplitude of magnetic (velocity) fluctuations $\delta B(f)$ ($\delta V(f)$) at a given frequency were computed considering that $\delta B(f)$ ($\delta V(f)$) and the Fourier power spectral density $P_B(f)$ ($P_V(f)$) are linked by the following relationship: $\delta B(f) = \sqrt{2fP_B(f)}$ (analogously for velocity fluctuations). $P_B(f)$ and $P_V(f)$ were computed from the trace of the power spectral density of B and V components, respectively, after smoothing each spectrum over 7 points. $\delta B(f)$ and $\delta V(f)$ were then normalized to the corresponding average magnitude of the velocity or magnetic field in the selected interval, as shown in Figure 2. In the panels below, the fast wind case (red) is compared to each Alfvénic slow wind stream (blue) both for velocity (left) and magnetic field (right) fluctuations.

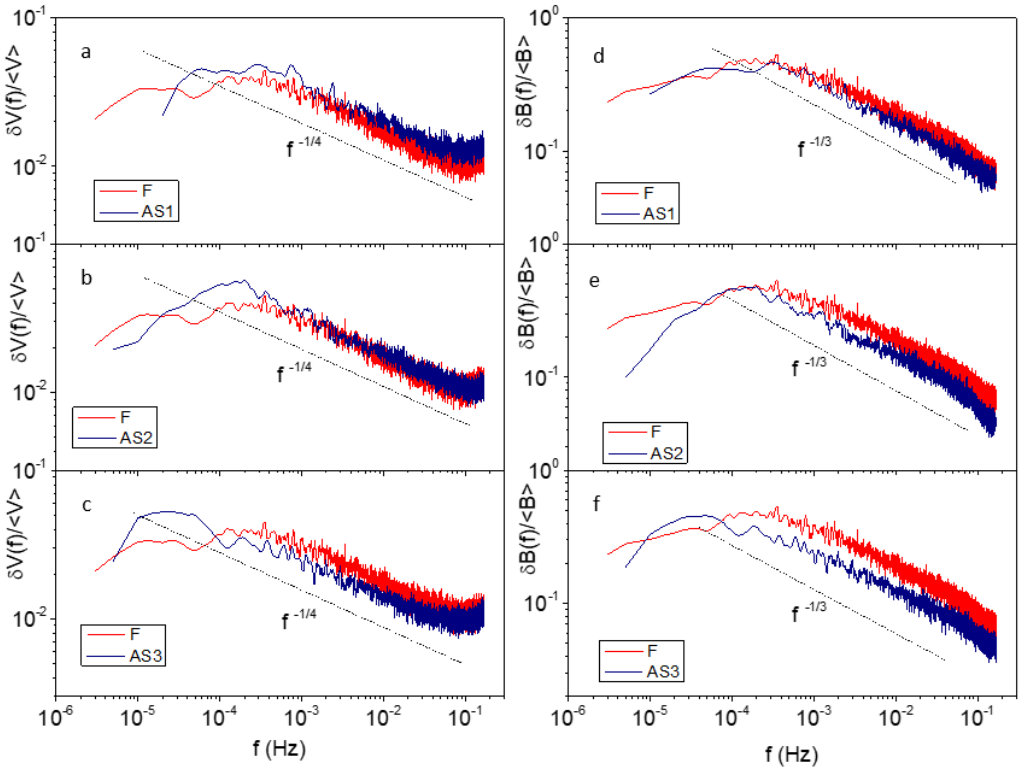

Figure 2. Normalized power spectral density of the trace of velocity (**a**–**c**) and magnetic field fluctuations (**d**–**f**) for fast wind (red, labeled F) and Alfvénic slow wind intervals (blue, labeled AS1, AS2 and AS3). The Kraichnan and Kolmogorov power laws, $f^{-1/4}$ and $f^{-1/3}$, respectively, are indicated as dashed lines.

Figure 2 shows that the normalized power associated with the trace of magnetic and velocity fluctuations is comparable to results displayed in [34]. It is worth noting, however, that each interval has different spectral behavior. Interval 'AS1' is characterized by slightly larger velocity fluctuations and slightly lower magnetic field fluctuations. $\delta V(f)/ < V >$ in interval 'AS2' superimposes on the same quantity related to the fast wind case while magnetic field fluctuations are slightly lower than the fast wind case. To conclude, the normalized spectra of V and B for interval 'AS3' are lower than the fast wind case. The result of this analysis and the ones in [34] suggest that, although the relative fluctuations in

the Alfvénic slow wind are larger than in the typical slow wind, each stream has a typical signature. This consideration can be extended to fast wind streams as well.

We recall that $\delta B(f)$ corresponding to the Kolmogorov scaling ($P_B(f) \sim f^{-5/3}$), is $f^{-1/3}$ while the Kraichnan scaling ($P_B(f) \sim f^{-3/2}$) is $f^{-1/4}$, both included as dashed lines in panel (**a**) and (**b**). The two scalings are usually invoked to reproduce the slope of the turbulent inertial range [31] that results to be closer to $f^{-5/3}$ for the magnetic field and closer to $f^{-3/2}$ for the velocity [41–44]. However, observations by Voyager have shown that the power spectrum of velocity fluctuations evolves toward a Kolmogorov scaling at heliocentric distances larger than 1 AU [23]. The flattening observed at low frequencies corresponds to the f^{-1} scaling, which has been interpreted as a saturated amplitude of the Fourier modes [40,45]. Although we do not intend to study in detail the location of the spectral break separating the f^{-1} and the inertial range, we observe that it is located around 2–3 $\times 10^{-4}$ Hz, in agreement with [34].

The Alfvénic content of the fluctuations can be investigated using the Elsässer variables [46], introduced for the first time in the analysis of interplanetary data by [4,47]. The Elsässer variables are defined as: $z^{\pm} = v \pm b$, where b is the magnetic field vector in Alfvén units, i.e., $b = B/\sqrt{\mu_0 \rho}$, with μ_0 the vacuum magnetic permeability, ρ the mass density evaluated taking into account both protons and alpha particles as $m_p(n_p + 4n_\alpha)$ (with n_α the alpha particles number density), and B the magnetic field vector. This definition refers to a background magnetic field pointing to the Sun, while $z^{\pm} = v \mp b$ holds for the opposite polarity. With these definitions, z^+ always corresponds to an outward propagation (with respect to the Sun) while z^- identifies inward-going fluctuations.

The total energy and the cross-helicity, which are invariants for the ideal Magnetohydrodynamic equations, can be expressed in terms of the Elsässer variables. In particular, we focus on the cross-helicity and derive the residual energy from the total energy. Indicating $e^{\pm}$ as the energy (per unit mass) associated to $z^{\pm}$ modes, and e^v and e^b the kinetic and magnetic energy (per unit mass), respectively, we can then define the normalized cross-helicity, $\sigma_C = (e^+ - e^-)/(e^+ + e^-)$, and the normalized residual energy, $\sigma_R = (e^v - e^b)/(e^v + e^b)$ [48]. σ_C and σ_R vary from -1 and +1, being normalized quantities. In particular, σ_C indicates the balance between z^+ and z^-, while σ_R is a measure of the balance between kinetic energy and magnetic energy (in Alfvén units). σ_C is equal to 1 (-1) if only the outward (inward) component is present, while absolute values below 1 correspond to a mixture of the two components and/or to non-Alfvénic fluctuations. The absence of magnetic (kinetic) fluctuations correspond to σ_R equal to +1 (-1), while equipartition gives $\sigma_R = 0$. The v-b correlation coefficient C_{vb} is related to σ_C by: $C_{vb} = \sigma_C / \sqrt{(1 - \sigma_R^2)}$ provided that $\sigma_R \neq \pm 1$ or, in other words, if both kinetic and magnetic fluctuations are present [23,49]. Therefore, C_{vb} and σ_C are coincident if $\sigma_R = 0$ namely, if there is balance between magnetic and kinetic energy. For a given value of C_{vb} a departure from the equipartition of energy leads to a reduction of σ_C. As a consequence, correlated v and b fluctuations of different amplitude (i.e., showing some energy imbalance) lead to $C_{vb} = 1$ and $0 < \sigma_C < 1$.

In the present analysis, we computed the power spectral density of the trace of z^+ and z^-, along with e^v and e^b and computed σ_C and σ_R in the frequency domain. Figure 3 shows the comparison between the fast (red) and the AS1 interval (blue), taken as an example. In particular, the top panel displays σ_C vs. frequency, while the middle and bottom panels show the power spectra of z^+ and z^- for the fast wind and the AS1 interval, respectively. It is worth noting that for frequencies below 10^{-3} Hz, the fast wind shows, in general, higher σ_C (apart from a peak in AS1 at 3×10^{-4} Hz) while for higher frequencies the behavior of σ_C is more similar in the two cases. It must be noted that the decrease of σ_C is linked to a flattening of e^- rather than a decrease of e^+ (see middle and bottom panels).

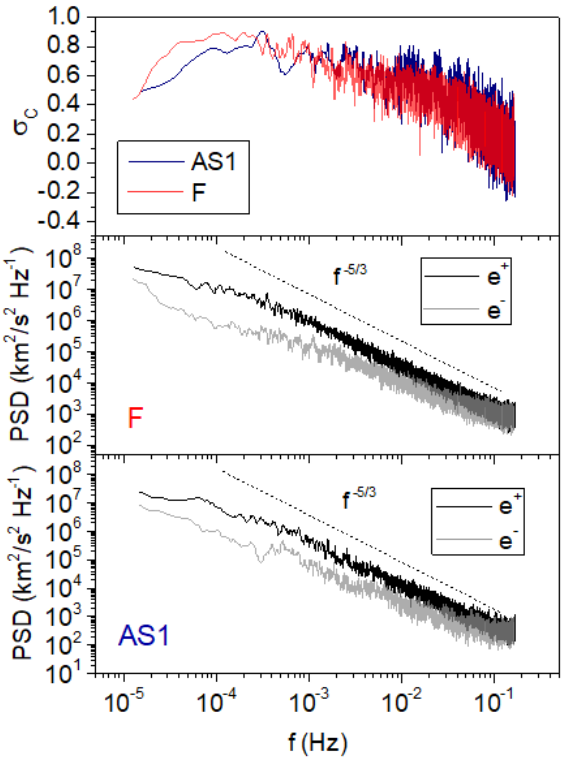

Figure 3. (**Top** panel) σ_C, vs. frequency referring to the main portion of the streams of the two solar wind intervals displayed in Figure 1, labeled F (red) and AS1 (blue), respectively. PSD of the trace of z^+ and z^- modes (e^+ and e^-, respectively) for the fast wind (**middle** panel) and for the Alfvénic slow wind (**bottom** panel).

Figure 4 shows similar plots for σ_R (top panel), e^v and e^b in middle and bottom panels for for fast and AS1, respectively. Both cases show an imbalance in favor of the magnetic energy with values in the range -0.35 to -0.2 for AS1 and -0.2 to -0.1 for the fast wind in the frequency range between 3×10^5 Hz and 0.04 Hz where σ_R values are more stable, avoiding the high-frequency part of the spectrum. Indeed, it must be noted that the tendency of σ_R to vanish and to an imbalance in favor of kinetic energy at higher frequencies is linked to a flattening of e^v, related to instrument noise (for frequencies $>$ 0.04 Hz), rather than a decrease of e^b. These results basically suggest that the fast stream is closer to equipartition of energy.

To corroborate our results, besides the comparison between F and AS1, we also included a comparison of σ_C and σ_R spectra between the fast stream (red) and the three Alfvénic slow streams (blue, from top to bottom panel: AS1, AS2, and AS3 in Figure 5).

Figure 5 confirms the previous findings and clearly suggests that, although being these streams somehow similar, they also show some peculiarities related to each stream. While the behavior of σ_C of AS2 overall is similar to the fast wind case, AS3 shows some frequencies below 10^{-3} Hz characterized by lower values of σ_C. The common feature that groups the three Alfvénic slow wind streams is the behavior of σ_R, showing always absolute σ_R greater than the fast wind (larger energy imbalance), while fast wind is generally closer to energy equipartition.

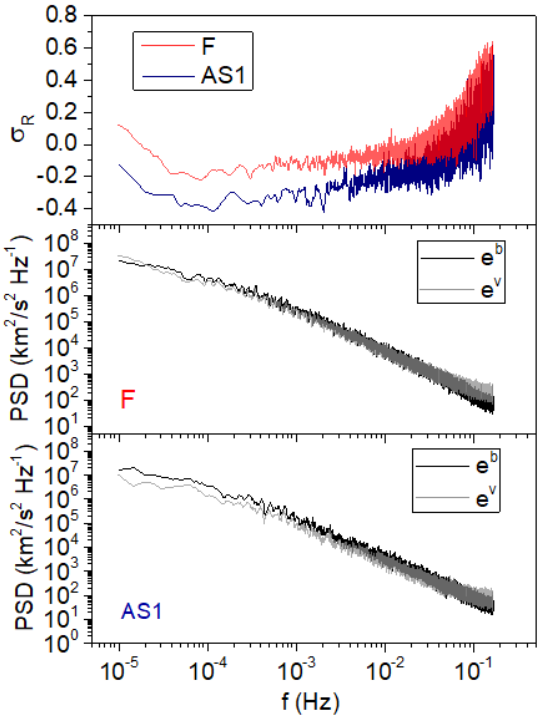

Figure 4. (**Top** panel) σ_R, vs. frequency referring to the main portion of the streams of the two solar wind intervals displayed in Figure 1, labeled F (red) and AS1 (blue), respectively. PSD of the trace of V and B (e^v and e^b, respectively) for the fast wind (**middle** panel, labeled F) and for the Alfvénic slow wind (**bottom** panel, labeled AS1).

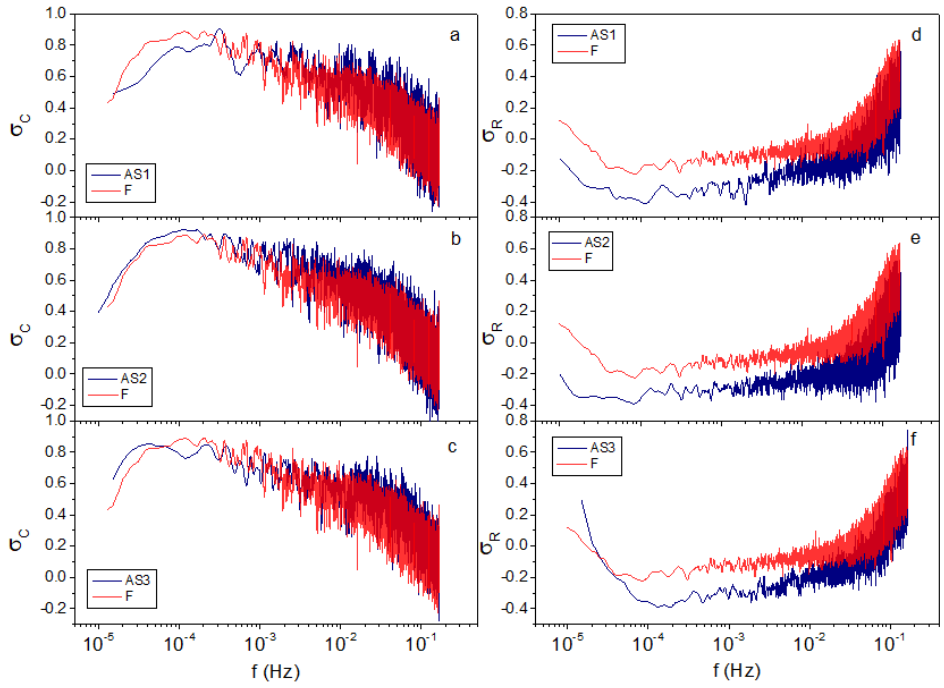

Figure 5. (**a**–**c**) Normalized cross-helicity, σ_C and (**d**–**f**) residual helicity, σ_R, vs. frequency for the three Alfvénic slow wind streams (blue, labeled AS1, AS2 and AS3) compared to the fast wind (red, labeled F).

4. Discussion and Concluding Remarks

In this study, we contributed to better characterize Alfvénic fluctuations in different solar wind streams comparing the behavior of different parameters. Alfvénic solar

wind streams can be identified basically by correlations between velocity and magnetic field components (high v-b correlation coefficient) [2] in the presence of incompressible conditions [4]. We studied C_{vb} along with the time series of the proton number density and magnetic field magnitude, of the relative amplitude of the magnetic field fluctuations with respect to the fluctuations in the magnitude, and the relative density amplitude with respect to the turbulent Mach number squared, to establish if the incompressible condition is satisfied. While high values of C_{vb} and $\delta b_i/\delta B > 1$ are robust conditions to identify Alfvénic intervals, our results show that further investigation is needed in order to understand to what extent the condition $\delta n_p/n_p < (\delta v/c_s)^2$ holds in solar wind displaying large-amplitude Alfvénic fluctuations. Indeed, comparing our findings with the results of a preliminary investigation on $\delta n_p/n_p$ and $(\delta v/c_s)^2$ in [15] for different Alfvénic intervals (fast and slow), we notice that the behavior of $\delta n_p/n_p$ respect to $(\delta v/c_s)^2$ in the Alfvénic slow wind shown in that paper at 1 AU is more similar to the fast wind of the present paper. Remarkably, when moving to PSP's first encounter, the two quantities are on average comparable in the selected interval. On the other hand, the dependence of this condition on the solar wind regime was investigated also by [4] using Helios data. In general, they found that the turbulent Mach number increases in fast flows and the relative amplitude of density fluctuations decreases to an order of magnitude lower, while the two quantities are comparable in the slower stream (which however are not Alfvénic). Similar results are found at two different scales.

The characterization of solar wind fluctuations can be performed by comparing the normalized power spectra for velocity and magnetic field. The result of this analysis along with the ones shown in [34] suggest that, although the relative fluctuations in the Alfvénic slow wind are larger than in the typical slow wind and then similar to those in the fast wind (in the same cases, the power of the fluctuations are superimposed), each stream has a typical signature. This remark stands also for different fast wind streams, not shown here.

In order to identify the scales that are Alfvénic we also studied the dependence of σ_C on frequency. Most Alfvénic scales range from tents of minutes to hours in agreement with previous studies [35]. Ref. [23] showed a depletion of σ_C for larger and larger time scales, that are then less and less Alfvénic. The depletion of the Alfvénic character of the outwardly propagating fluctuations, within the hourly frequency range, was investigated by [50] who suggested that a role might be played by the interaction between Alfvénic fluctuation with static structures or magnetosonic perturbations able to modify the homogeneity of the background medium on a scale size comparable with the wavelength of the fluctuations. This issue deserves further investigation. On the other hand, we observe a decrease of σ_C for small scales (high frequencies) that depends on the flattening of e^- rather than a decrease of e^+.

Moreover, we studied the spectra of σ_R to evaluate the energy balance of solar wind fluctuations at different scales. In principle, σ_R should be close to 0 (indicating equipartition between kinetic and magnetic energy) in Alfvénic intervals. However, our findings showed that there is an imbalance in favor of the magnetic energy which is confirmed by previous studies. Indeed, [51] observed the same behavior in σ_R (in terms of the Alfvén ratio r_A, which is the ratio between kinetic energy and magnetic energy in Alfvén units, e^v/e^b, and linked to σ_R by $(r_A - 1)/(r_A + 1)$), a distance close to 1 AU using Helios data. Refs. [2,22,52] showed that r_A is usually less than unit and reaches a limit value around 0.45 at some AU and then stabilizes [22,53], thus determining a limit value also for σ_R around -0.38, well in agreement with our findings, although the fast wind stream is closer to energy equipartition than the Alfvénic slow wind intervals. The behavior of σ_R to be different from 0 is still an open issue. Although numerical simulations predict $r_A < 1$ [54,55] that may be due to the Alfvén effect [56] competing with a local dynamo effect [4,57,58], it would predict general values of $r_A \neq 1$ resulting also in a final excess of kinetic energy. Although corrections have been suggested to take into account the role played by the presence of alpha particles, or anisotropy in the thermal pressure [2] or the three fluid effects [59], these are not able to explain the observed depletion of r_A thus

suggesting that it might be due to a natural evolution of turbulence determining a state dominated by magnetic energy [4,55,60,61] or, it might be due to the high occurrence of magnetic structures as the ones described by [62].

Refs. [44,63,64] studied the scaling of the power spectra of the cross-helicity ($H_c = e^+ - e^-$), the residual energy ($E_r = e^v - e^b$) and the total energy ($E_{tot} = e^v + e^b$) finding that while the slope of E_r is close to $-5/3$, that of E_{tot} and H_c are much closer to $-3/2$. In particular, [63] found that the spectral index of E_{tot} is a function of σ_C, varying from roughly $5/3$ when $\sigma_C \approx 0$ to approximately $3/2$ when $\sigma_C \approx 1$. Moreover, the same authors found that E_{tot} and H_c spectra are usually well correlated in the inertial range. We performed a similar analysis on F, AS1, AS2, and AS3 (not shown here) basically confirming these scalings. As highlighted by [64], the scaling of E_{tot} is related to the residual energy of the solar wind. Indeed, correspondence is found between magnetically dominated intervals, with $\sigma_R \approx -1$, and steeper magnetic spectra. When $\sigma_R \approx -1$, the magnetic energy dominates the kinetic energy; accordingly, the total energy is approximately equal to the magnetic energy (close to $5/3$). When there is equipartition between kinetic and magnetic energy, the scalings of kinetic and magnetic energy spectra are similar and the scaling of the total energy is close to $3/2$. The same authors suggested that the observed difference between the spectral indices of velocity and magnetic field turbulent fluctuations is due to the presence of negative residual energy caused by intermittent events (e.g., current sheets) in the magnetic field that are not accompanied by signature in the velocity fluctuations. Within this context, the different residual energy characterizing fast and Alfvénic slow streams would suggest a different content of intermittent structures. This aspect should be further investigated since intermittency has not yet been studied in Alfvénic slow streams.

This study basically confirms similarities between fast and slow wind streams provided that the latter are Alfvénic. Moreover, the results of this paper suggest that, despite the similarities between fast wind and Alfvénic slow wind streams, each stream shows also peculiar features, that can be linked to the intrinsic evolution history that each of them has experienced and that should be taken into account. Since several questions remain still open, further studies are needed, aimed at investigating a larger number of Alfvénic streams and the dependence of the quantities studied in the paper on the scale.

The characterization of the Alfvénic turbulence in the Alfvénic slow wind is extremely important to interpret future observations of the same solar wind regime and, to a large extent, to improve our understanding of the general problem of solar wind acceleration. Although our results, compared to previous findings at 1 AU, suggest that the Alfvénic slow wind might undergo an evolution similar to the fast wind [65], with large amplitude Alfvénic fluctuations evolving towards a state of smaller amplitude and less Alfvénic fluctuations and growing magnetic energy excess [66], it is still unclear why the Alfvénic content of the fluctuations we find to be dominant close to the Sun (at Helios perihelion and closer to the Sun with PSP) in slow streams appear to be rapidly lost by 1 AU, in most cases, while surviving in other cases, e.g., [15].

This is why it is particularly relevant to study solar wind Alfvénicity with PSP and Solar Orbiter. While PSP will provide information on the solar wind in the immediate surroundings of the Sun, Solar Orbiter will contribute to identifying the solar source of the Alfvénic slow wind and the link with plasma properties in the interplanetary medium. Launched in August 2018 and February 2020, respectively, during the minimum of solar cycle 24, the two missions will indeed be in operation during the maximum of solar cycle 25 that is expected to peak between 2023 and 2026. This phase of the solar cycle is particularly interesting for our purpose since it is characterized by a higher incidence of the Alfvénic slow wind, as derived from previous studies, due to a higher occurrence of overexpanded open field regions on the solar surface. Future observations will then be crucial to study Alfvénic slow wind streams identified in alignments of the two spacecraft or same stream crossings by the same spacecraft for PSP [67]. The sampling of solar wind from the same solar sources at different radial distances or in consecutive solar rotations will help to elucidate how and why Alfvénicity in the solar wind evolves in the inner heliosphere.

Author Contributions: Conceptualization, R.D. and M.V.; Formal analysis, R.D.; Investigation, R.D. and D.P.; Methodology, R.D.; Writing—original draft, R.D.; Writing—review and editing, R.D., D.P., M.V., L.S.-V., D.T., R.B. and R.D.M. All authors have read and agreed to the published version of the manuscript.

Funding: This research received no external funding.

Data Availability Statement: Data are available in the NASA-CDAWeb website: https://cdaweb.sci.gsfc.nasa.gov.

Acknowledgments: The authors acknowledge R. Lin (UC Berkeley) and R. P. Lepping (NASA/GSFC) for the provision of WIND/3DP and WIND/MFI data, respectively.

Conflicts of Interest: The authors declare no conflict of interest.

References

1. Coleman, P.J. Turbulence, Viscosity, and Dissipation in the Solar-Wind Plasma. *Astroph. J.* **1968**, *153*, 371–388. [CrossRef]
2. Belcher, J.W.; Davis, L. Large-amplitude Alfvén waves in the interplanetary medium, 2. J. Geophys. Res. **1971**, *76*, 3534. [CrossRef]
3. Belcher, J.W.; Solodyna, C.V. Alfvén waves and directional discontinuities in the interplanetary medium. *J. Geophys. Res.* **1975**, *80*, 181. [CrossRef]
4. Grappin, R.; Velli, M.; Mangeney, A. "Alfvénic" versus "standard" turbulence in the solar wind. *Ann. Geophys.* **1991**, *9*, 416–426.
5. Lighthill, M.J. On Sound Generated Aerodynamically. II. Turbulence as a Source of Sound. *Proc. R. Soc. Lond. A* **1954**, *222*, 1148.
6. Bavassano, B.; Bruno, R. Density fluctuations and turbulent Mach numbers in the inner solar wind. *J. Geophys. Res.* **1995**, *100*, 9475–9480. [CrossRef]
7. Marsch, E.; Mülhäuser, K.-H.; Schwenn, R.; Rosenbauer, H.; Pilipp, W.; Neubauer, F.M. Solar Wind Protons' Three-Dimensional Velocity Distributions and Derived Plasma Parameters Measured Between 0.3 and 1 AU. *J. Geophys. Res.* **1982**, *87*, 52–72. [CrossRef]
8. Kolmogorov, A.N. The Local Structure of Turbulence in Incompressible Viscous Fluid for Very Large Reynolds' Numbers. *Akad. Nauk SSSR Dokl.* **1941**, *30*, 301
9. Marsch, E.; Mühlhäuser, K.-H.; Rosenbauer, H.; Schwenn, R.; Denskat, K.U. Pronounced proton core temperature anisotropy, ion differential speed, and simultaneous Alfvén wave activity in slow solar wind at 0.3 AU. *J. Geophys. Res.* **1981**, *86*, 9199. [CrossRef]
10. D'Amicis, R.; Bruno, R.; Bavassano, B. Response of the geomagnetic activity to solar wind turbulence during solar cycle 23. *J. Atm. Sol.-Terr. Phys.* **2011**, *73*, 653. [CrossRef]
11. D'Amicis, R.; Bruno, R. On the origin of highly Alfvénic slow solar wind. *Astropys. J.* **2015**, *805*, 84. [CrossRef]
12. D'Amicis, R.; Matteini, L.; Bruno, R. On the slow solar wind with high Alfvénicity: From composition and microphysics to spectral properties. *Mon. Not. R. Astron. Soc.* **2019**, *483*, 4665. [CrossRef]
13. Perrone, D.; D'amicis, R.; De Marco, R.; Matteini, L.; Stansby, D.; Bruno, R.; Horbury, T.S. Highly Alfvénic slow solar wind at 0.3 au during a solar minimum: Helios insights for Parker Solar Probe and Solar Orbiter. *Astron. Astrophys.* **2020**, *633*, A166. [CrossRef]
14. Stansby, D.; Matteini, L.; Horbury, T.S.; Perrone, D.; D'Amicis, R.; Berčič, L. The origin of slow Alfvénic solar wind at solar minimum. *Mon. Not. R. Astron. Soc.* **2020**, *492*, 39. [CrossRef]
15. D'Amicis, R.; Perrone, D.; Bruno, R.; Velli, M. On Alfvénic slow wind: A journey from the Earth back to the Sun. *J. Geophys. Res.* **2021**, *126*, e2020JA028996. [CrossRef]
16. Bale, S.D.; Badman, S.T.; Bonnell, J.W.; Bowen, T.A.; Burgess, D.; Case, A.W.; Cattell, C.A.; Chandran, B.D.G.; Chaston, C.C.; Chen, C.H.K.; et al. Highly structured slow solar wind emerging from an equatorial coronal hole. *Nature* **2019**, *576*, 237. [CrossRef]
17. Kasper, J.C.; Bale, S.D.; Belcher, J.W.; Berthomier, M.; Case, A.W.; Chandran, B.D.G.; Curtis, D.W.; Gallagher, D.; Gary, S.P.; Golub, L.; et al. Alfvénic velocity spikes and rotational flows in the near-sun solar wind. *Nature* **2019**, 576, 228. [CrossRef]
18. Parashar, T.N.; Goldstein, M.L.; Maruca, B.A.; Matthaeus, W.H.; Ruffolo, D.; Bandyopadhyay, R.; Chhiber, R.; Chasapis, A.; Qudsi, R.; Vech, D.; et al. Measures of scale-dependent Alfvénicity in the first PSP solar encounter. *Astropys. J.* **2020**, *246*, 58 [CrossRef]
19. D'Amicis, R.; Bruno, R.; Panasenco, O.; Telloni, D.; Perrone, D.; Marcucci, M.F.; Woodham, L.; Velli, M.; De Marco, R.; Jagarlamudi, V.; et al. First Solar Orbiter observation of the Alfvénic slow wind and identification of its solar source. *Astron. Astrophys.* **2021**, 656, A21 [CrossRef]
20. Panasenco, O.; Velli, M. Coronal pseudostreamers: Source of fast or slow solar wind? *AIP Conf. Proc.* **2013**, *1539*, 50–53.
21. Panasenco, O.; Velli, M.; Panasenco, A. Large-scale Magnetic Funnels in the Solar Corona. *Astrophys. J.* **2019**, *873*, 25. [CrossRef]
22. Matthaeus, W.H.; Goldstein, M.L. Measurement of the rugged invariants of magnetohydrodynamic turbulence in the solar wind. *J. Geophys. Res.* **1982**, *87*, 6011. [CrossRef]
23. Roberts, D.A.; Klein, L.W.; Goldstein, M.L.; Matthaeus, W.H. The nature and evolution of magnetohydrodynamic fluctuations in the solar wind: Voyager observations. *J. Geophys. Res.* **1987**, *92*, 11021. [CrossRef]
24. Roberts, D.A.; Goldstein, M.L.; Klein, L.W.; Matthaeus, W.H. Origin and evolution of fluctuations in the solar wind: Helios observations and Helios-Voyager comparisons. *J. Geophys. Res.* **1987**, *92*, 12023. [CrossRef]
25. Grappin, R.; Velli, M. Waves and streams in the expanding solar wind. *J. Geophys. Res.* **1996**, *101*, 425. [CrossRef]

26. Bavassano, B.; Pietropaolo, E.; Bruno, R. Alfvénic turbulence in the polar wind: A statistical study on cross helicity and residual energy variations. *J. Geophys. Res.* **2000**, *105*, 12697. [CrossRef]
27. Matthaeus, W.H.; Minnie, J.; Breech, B.; Parhi, S.; Bieber, J.W.; Oughton, S. Transport of cross helicity and radial evolution of Alfvénicity in the solar wind. *Geophys. Res. Lett.* **2004**, *31*, L12803. [CrossRef]
28. Bavassano, B.; Bruno, R. Evidence of local generation of Alfvénic turbulence in the solar wind. *J. Geophys. Res.* **1989**, *94*, 11977. [CrossRef]
29. Bavassano, B.; Bruno, R. Large-scale solar wind fluctuations in the inner heliosphere at low solar activity. *J. Geophys. Res.* **1989**, *94*, 168. [CrossRef]
30. Bruno, R.; Bavassano, B. Origin of low cross-helicity regions in the inner solar wind. *J. Geophys. Res.* **1991**, *96*, 7841 [CrossRef]
31. Bruno, R.; Carbone, V. The Solar Wind as a Turbulence Laboratory. *Living Rev. Sol. Phys.* **2013**, *10*, 2. [CrossRef]
32. Panasenco, O.; Velli, M.; D'Amicis, R.; Shi, C.; Réville, V.; Bale, S.D.; Badman, S.T.; Kasper, J.; Korreck, K.; Bonnell, J.W. Exploring solar wind origins and connecting plasma flows from the Parker Solar Probe to 1 AU: Nonspherical source surface and Alfvénic fluctuations. *Astrophys. J.* **2020**, *246*, 54. [CrossRef]
33. D'Amicis, R.; Alielden, K.; Perrone, D.; Bruno, R.; Telloni, D.; Raines, J.M.; Lepri, S.T.; Zhao, L. Solar wind Alfvénicity during solar cycle 23 and 24. Perspective for future observations with Parker Solar Probe and Solar Orbiter. *Astron. Astrophys.* **2021**, *654*, A111. [CrossRef]
34. D'Amicis, R.; Matteini, L.; Bruno, R.; Velli, M. Large amplitude fluctuations in the Alfvénic solar wind. *Sol. Phys.* **2020**, *295*, 46. [CrossRef]
35. Marsch, E.; Tu, C.-Y. On the radial evolution of MHD turbulence in the Inner heliosphere. *J. Geophys. Res.* **1990**, *95*, 8122. [CrossRef]
36. Neugebauer, M.; Goldstein, B.E.; McComas, D.J.; Suess, S.T.; Balogh, A. Ulysses observations of microstreams in the solar wind from coronal holes. *J. Geophys. Res.* **1995**, *100*, 23389. [CrossRef]
37. Neugebauer, M.; Ruzmaikin, A.; McComas, D.J. Wavelet analysis of the structure of microstreams in the polar solar wind. *AIP Conf. Proc.* **1997**, *385*, 41.
38. Horbury, T.S.; Matteini, L.; Stansby, D. Short, large-amplitude speed enhancements in the near-Sunfast solar wind. *Mon. Not. R. Astron. Soc.* **2018**, *478*, 1980. [CrossRef]
39. Neugebauer, M. Evidence for Polar X-Ray Jets as Sources of Microstream Peaks in the Solar Wind. *Astrophys. J.* **2012**, *750*, 2012. [CrossRef]
40. Bruno, R.; Telloni, D.; Sorriso-Valvo, L.; Marino, R.; De Marco, R.; D'Amicis, R.R. The low-frequency break observed in the slow solar wind magnetic spectra. *Astron. Astrophys.* **2019**, *627*, A96. [CrossRef]
41. Podesta, J.J.; Roberts, D.A.; Goldstein, M.L. Power spectrum of smallscale turbulent velocity uctuations in the solar wind. *J. Geophys. Res.* **2006**, *111*, A10109. [CrossRef]
42. Podesta, J.J.; Roberts, D.A.; Goldstein, M.L. Spectral exponents of kinetic and magnetic energy spectra in solar wind turbulence. *Astrophys. J.* **2007**, *664*, 543. [CrossRef]
43. Salem, C.; Mangeney, A.; Bale, S.D.; Veltri, P. Solar wind magnetohydrodynamics turbulence: Anomalous scaling and role of intermittency. *Astrophys. J.* **2009**, *702*, 537. [CrossRef]
44. Borovsky, J.E. The velocity and magnetic field fluctuations of the solar wind at 1 AU: Statistical analysis of Fourier spectra and correlations with plasma properties. *J. Geophys. Res.* **2012**, *117*, A05104. [CrossRef]
45. Matteini, L.; Stansby, D.; Horbury, T.S.; Chen, C.H.K. On the 1/f Spectrum in the Solar Wind and Its Connection with Magnetic Compressibility. *Astrophs. J. Lett.* **2018**, *869*, L32. [CrossRef]
46. Elsässer, W.M. The Hydromagnetic Equations. *Phys. Rev.* **1950**, *79*, 183. [CrossRef]
47. Tu, C.-Y.; Marsch, E.; Thieme, K.M. Basic properties of solar wind MHD turbulence near 0.3 AU analyzed by means of Elsässer variables. *J. Geophys. Res.* **1989**, *94*, 11739. [CrossRef]
48. Tu, C.-Y.; Marsch, E. MHD structures, waves and turbulence in the solar wind: Observations and theories. *Space Sci. Rev.* **1995**, *73*, 1. [CrossRef]
49. Grappin, R.; Frisch, U.; Léorat, J.; Pouquet, A. Alfvenic fluctuations as asymptotic states of MHD turbulence. *Astron. Astrophys.* **1982**, *105*, 6.
50. Bruno, R.; Bavassano, B. Cross-helicity depletions in the inner heliosphere, and magnetic field and velocity fluctuation decoupling. *Plan. Space Sci.* **1993**, *41*, 677. [CrossRef]
51. Bruno, R.; Bavassano, B.; Villante, U. Evidence for long period Alfvén waves in the inner solar system. *J. Geophys. Res.* **1985**, *90*, 4373. [CrossRef]
52. Solodyna, C.V.; Belcher, J.W. On the minimum variance direction of magnetic field fluctuations in the azimuthal velocity structure of the solar wind. *Geophys. Res. Lett.* **1976**, *3*, 565 [CrossRef]
53. Roberts, D.A.; Goldstein, M.L.; Klein, L.W. The amplitudes of interplanetary fluctuations: Stream structure, heliocentric distance, and frequency dependence. *J. Geophys. Res.* **1990**, *95*, 4203. [CrossRef]
54. Matthaeus, W.H. The Alfvén effect reconsidered. In *1986 Sherwood Controlled Fusion Theory Conference*; Courant Institute of Mathematical Sciences: New York, NY, USA, 1986.
55. Mininni, P.D.; Gómez, D.O.; Mahajan, S.M. Dynamo Action in Magnetohydrodynamics and Hall-Magnetohydrodynamics. *Astrophys. J.* **2003**, *587*, 472. [CrossRef]

56. Kraichnan, R.H. Inertial-Range Spectrum of Hydromagnetic Turbulence. *Phys. Fluids* **1965**, *8*, 1385. [CrossRef]
57. Grappin, R.; Leorat, J.; Pouquet, A. Dependence of MHD turbulence spectra on the velocity field-magnetic field correlation. *Astron. Astrophys.* **1983**, *126*, 51–58.
58. Müller, W.-C.; Grappin, R. Spectral Energy Dynamics in Magnetohydrodynamic Turbulence. *Phys. Rev. Lett.* **2005**, *95*, 114502. [CrossRef]
59. Bavassano, B.; Bruno, R. Velocity and magnetic field fluctuations in Alfvénic regions of the inner solar wind: Three-fluid observations. *J. Geophys. Res.* **2000**, *105*, 51135118. [CrossRef]
60. Roberts, D.A.; Goldstein, M.L.; Matthaeus, W.H.; Ghosh, S. Velocity Shear Generation of Solar Wind Turbulence. *J. Geophys. Res.* **1992**, *97*, 17115–17130. [CrossRef]
61. Roberts, D.A. Observation and simulation of the radial evolution and stream structure of solar wind turbulence. In *Solar Wind Seven, Proceedings of the 3rd COSPAR Colloquium, Goslar, Germany, 16–20 September 1991*; COSPAR Colloquia Series; Marsch, E., Schwenn, R., Eds.; Pergamon Press: Oxford, UK; New York, NY, USA, 1992; pp. 533–538.
62. Tu, C.-Y.; Marsch, E. A model of solar wind fluctuations with two components:Alfvén waves and convective structures. *J. Geophys. Res.* **1993**, *98*, 1257–1276. [CrossRef]
63. Podesta, J.J.; Borovsky, J.E. Scale invariance of normalized cross-helicity throughout the inertial range of solar wind turbulence. *Phys. Plasmas* **2010**, *17*, 112905. [CrossRef]
64. Bowen, T.A.; Mallet, A.; Bonnell, J.W.; Bale, S.D. Impact of Residual Energy on Solar Wind Turbulent Spectra. *Astrophy. J.* **2018**, *865*, 45. [CrossRef]
65. Bavassano, B.; Dobrowolny, M.; Mariani, F.; Ness, N.F. Radial evolution of power spectra of interplanetary Alfvénic turbulence. *J. Geophys. Res.* **1982**, *87*, 3617. [CrossRef]
66. Bruno, R.; D'Amicis, R.; Bavassano, B.; Carbone, V.; Sorriso-Valvo, L. Magnetically dominated structures as an important component of the solar wind turbulence. *Ann. Geophys.* **2007**, *25*, 1913. [CrossRef]
67. Velli, M.; Harra, L.K.; Vourlidas, A.; Schwadron, N.; Panasenco, O.; Liewer, P.C.; Müller, D.; Zouganelis, I.; Cyr, O.C.S.; Gilbert, H.; et al. Understanding the origins of the heliosphere: Integrating observations and measurements from Parker Solar Probe, Solar Orbiter, and other space- and ground-based observatories. *Astron. Astrophys.* **2020**, *642*, A4. [CrossRef]